*Paleoclimatology and Paleoceanography*

Supporting Information for

# Early Pleistocene obliquity-scale $pCO_2$ variability at ~1.5 million years ago

Kelsey A. Dyez[1]*, Bärbel Hönisch[1,2], Gavin A. Schmidt[3]

[1]Lamont-Doherty Earth Observatory, Columbia University, Palisades, NY, USA.
[2]Department of Earth and Environmental Sciences of Columbia University, New York, NY, USA
[3]NASA Goddard Institute for Space Studies, New York, NY, USA

*kdyez@umich.edu

**Contents of this file**

Introduction
Figures S1 to S9
Tables S1 to S2

**Additional data files**

Tables S3 and S4 (xlsx),
data also archived at NOAA (NCEI)

## Introduction

The supplemental appendix contains additional supporting information, figures, and tables, in the same order as each is discussed in the main text. These figures provide supporting information for the choice of the $\delta^{11}B_{sw}$ value (Figure S1), alkalinity (Figure S2), and the chronology for Site 668B (Figure S3). They provide additional comparisons with previous work (Figures S4, S5), and plots of supplemental data (Figures S6, S7, S8).

### Pliocene salinity estimates

In section 2.7, Plio-Pleistocene salinity was estimated from a model of sea level changes and assumed to be constant for samples prior to 3 Ma. An alternative method for estimating salinity is via $\delta^{18}O_{calcite}$ and SST estimates [*Bemis et al.*, 1998]. For Site 999A, this alternative relies on planktic $\delta^{18}O$ measurements [*Schmidt et al.*, 2004] and Mg/Ca-based SST [*Schmidt et al.*, 2004; *Martínez-Botí et al.*, 2015], via the following equations:

$\delta^{18}O_{sw} = (SST - 16.5)/4.8 + \delta^{18}O_{calcite} + 0.27$ [*Bemis et al.*, 1998]
$Salinity = (\delta^{18}O_{sw\ Caribbean} + 10.511) / 0.319$ [*Steph et al.*, 2006]

This alternative method results in salinity that is on average within ±0.5‰ of the method used in the manuscript, but exhibits larger swings in salinity (>2‰) that are difficult to reconcile with

the smaller amplitude of sea level change (<25 m) in the Pliocene [*Hansen et al.*, 2013]. In practice, salinity variations have only a small impact on the pH estimate from boron isotopes (salinity ±1‰ = ±0.006 pH units). To account for the glacial-interglacial uncertainty on this estimate, a salinity uncertainty of ±2‰ is propagated through the pH and $pCO_2$ uncertainty calculations.

Model equations

In section 4.3, a simple box model is presented to relate ice volume, temperature, and carbon dioxide levels. This model does not have explicit geography, topography, or circulation; the governing equations are as follows:

$$\tau_L \frac{dL}{dt} = F_I + (aT - L)$$

$$\tau_C \frac{dC}{dt} = bT - C)$$

$$\frac{dT}{dt} = \mu L + F_{CO2}(C) + \lambda T - P(T, T_0) + \varepsilon$$

where, in the first equation, $F_I$ is the forcing of ice sheets and $\tau_L$ is a time constant for the ice sheet response. Similarly, in the second equation, $b$ is the carbon cycle sensitivity to temperature and $\tau_C$ is the response time. In the third equation, $\mu$ is the radiative forcing associated with the ice sheets, $\lambda$ is the non-Planck feedback and ε is a small source of random noise. For further documentation and discussion of this model, see the supplementary material of *Schmidt et al.* [2017].

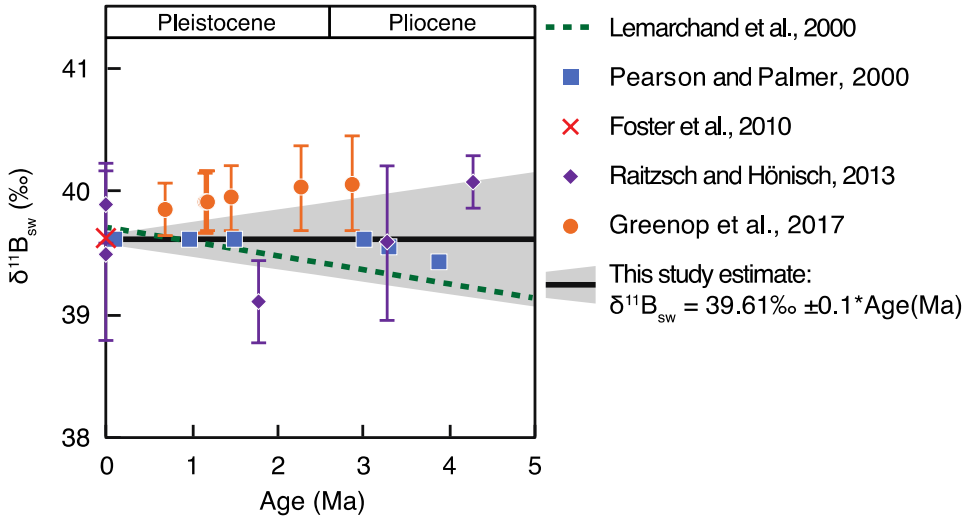


**Figure S1**. Compilation of $\delta^{11}B_{sw}$ estimates from previous work. Seawater $\delta^{11}B$ has been reconstructed from a model from river inputs [*Lemarchand et al.*, 2000], benthic foraminiferal $\delta^{11}B$ alongside modeled ocean pH [*Raitzsch and Hönisch*, 2013], and multi-species foraminiferal $\delta^{11}B$ measurements in the water column coupled with the water column pH gradient [*Pearson and Palmer*, 2000; *Greenop et al.*, 2017]. The estimates of *Pearson and Palmer* [2000] have been offset by +0.51‰ so that modern $\delta^{11}B_{sw}$ is equal to 39.61‰ [*Foster et al.*, 2010]. The $\delta^{11}B_{sw}$ value used in this study is the solid line (constant at the modern value) with uncertainty increasing with time (±0.1‰/Myr), which is depicted by the gray band.

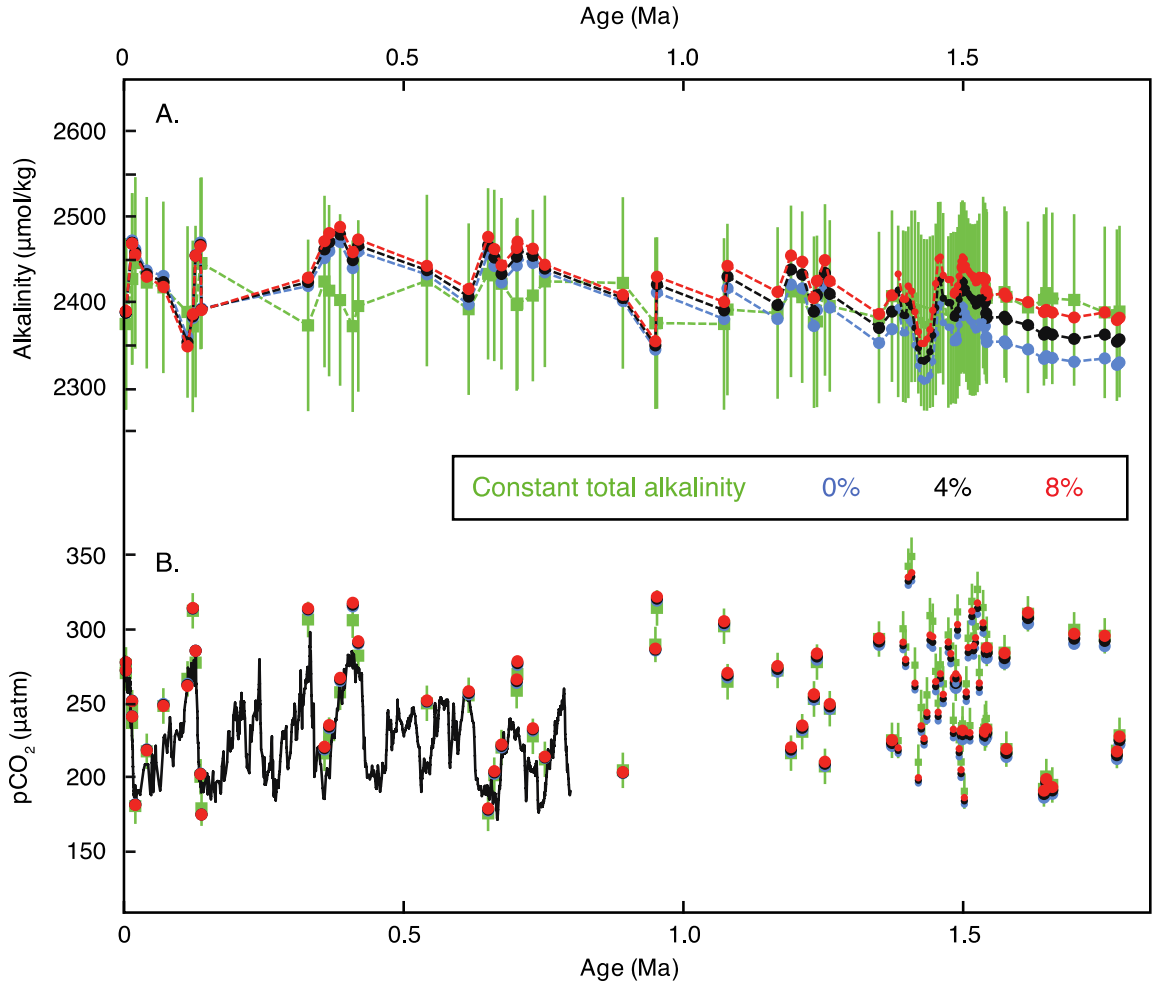


**Figure S2**. Comparison of various alkalinity scenarios used to estimate $pCO_2$ from Site 668B. (A) Alkalinity estimates for 4 scenarios; green squares represent 'constant total alkalinity' in which alkalinity is scaled as a function of sea level; the uncertainty band is ±100 µmol/kg. Blue, black, and red circles represent scenarios in which continental weathering, calcite production, and seafloor dissolution impact ocean alkalinity after the geochemical model of *Clark et al*. [2006]. Alkalinity was estimated from this same model in the study of *Hönisch et al*. [2009], although the time axis of the model alkalinity output was erroneously reversed in that study. The $pCO_2$ estimates we derive here are nearly the same as the original publication, which reflects the small influence alkalinity has on the $pCO_2$ estimate when alkalinity differs by less than 200 µmol/kg. The difference between the other estimates reflects the relative contribution of Canadian Shield weathering to global weathering rates (blue = 0%, black = 4%, red = 8%). The average absolute value of the difference between the 0% scenario and the constant alkalinity scenario is 33 µmol/kg . (B) Comparison of $pCO_2$ calculated via the different alkalinity scenarios compared to ice core $pCO_2$ [*Bereiter et al.*, 2015]. The impact of the varying alkalinity scenarios on calculated $pCO_2$ values is smaller than the uncertainty in the constant total alkalinity scenario (±100 µmol/kg); the largest difference in calculated $pCO_2$ between any varying alkalinity scenario and the 'constant total alkalinity' scenario is 12 µatm. Uncertainty in the lower panel is only due to alkalinity in the constant total alkalinity scenario ($2\sigma$).

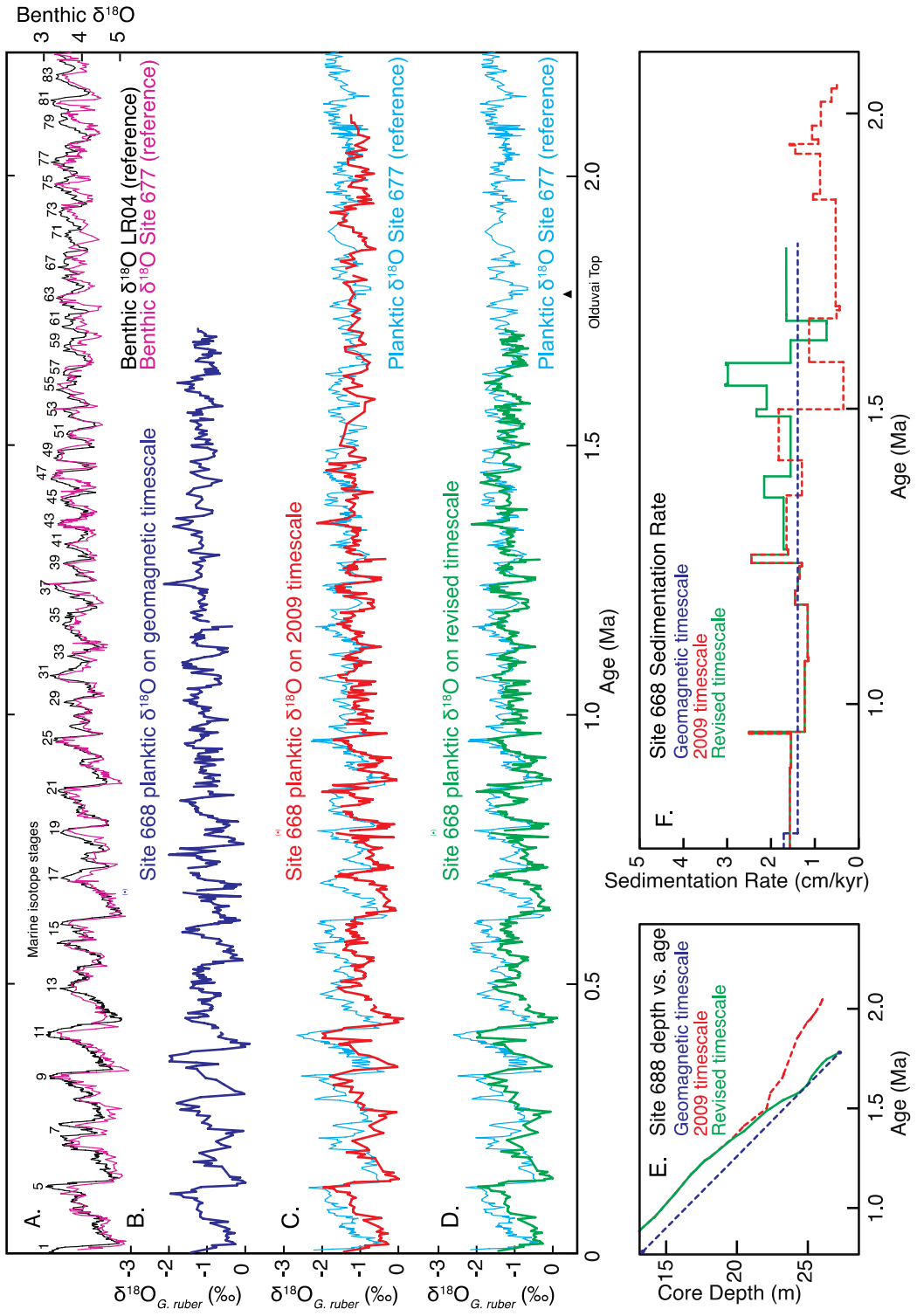


**Figure S3**. Comparison of published and revised age model for Site 668B. (A) Reference curves are the benthic $\delta^{18}O$ stack (black line) [*Lisiecki and Raymo*, 2005] and benthic $\delta^{18}O$ from Site 677 (magenta line) [*Shackleton et al.*, 1990]. (B) Site 688B planktic $\delta^{18}O$ plotted using the

original timescale from ODP initial reports, which relied on geomagnetic estimates and microfossil appearances [*Shipboard Scientific Party*, 1988]. (C) Site 688B planktic $\delta^{18}O$ plotted using the published '2009 timescale' (red line) [*Hönisch et al.*, 2009], which was based on visual alignment of the Site 668B planktic $\delta^{18}O$ record with both the Site 677 planktic $\delta^{18}O$ record (light blue line) [*Shackleton et al.*, 1990] and the LR04 benthic $\delta^{18}O$ stack [*Lisiecki and Raymo*, 2005]. (D) Site 668B planktic $\delta^{18}O$ plotted using the revised timescale (green line), which remains the same as the previously published '2009 timescale' for ages 0-1.3 Ma and is only adjusted for ages prior to 1.3 Ma. Revisions are made in AnalySeries [*Paillard et al.*, 1996] based on visual alignment of the Site 668B planktic $\delta^{18}O$ record with the Site 677 planktic $\delta^{18}O$ record and using the top of the Olduvai magnetic reversal as an additional tie point (core depth 27.2-27.3 m; 1.78 Ma [*Shipboard Scientific Party*, 1988]). (E) The depth vs. age comparison for the revised timescale for Site 668B. (F) Using the revised timescale, sedimentation rate for Site 668B varied between 0.7 and 3.0 cm/kyr.

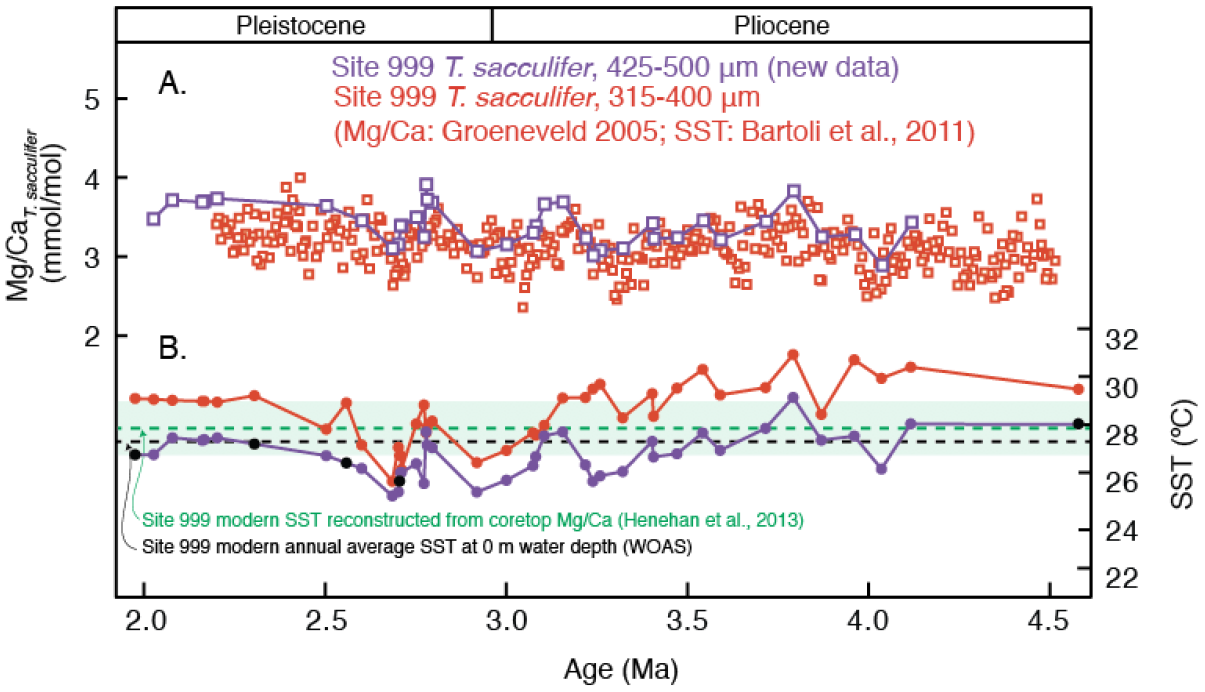


**Figure S4**. (A) Site 999A *T. sacculifer* (425-500 µm) measured Mg/Ca values (open purple squares) from the same or adjacent samples to those with boron isotope measurements from *Bartoli et al*. [2011]. The original *T. sacculifer* Mg/Ca record [*Groeneveld*, 2005] used by *Bartoli et al*. [2011] is plotted for reference (open red squares). The new Mg/Ca data are slightly higher and from the same larger size fraction also used for $\delta^{11}B$. (B) The new SST estimate (filled purple circles) is then calculated using the new Mg/Ca data and applying an upward adjustment by +10% due to our use of the reductive cleaning step, which has been reported to lower the Mg/Ca value by 10% [*Martin and Lea*, 2002]. The new SST record is corrected for changes in $Mg/Ca_{sw}$ using the approach of *Medina-Elizalde et al*. [2008] and a modern $Mg/Ca_{sw}$ value of 5.2 mmol/mol [*Evans and Müller*, 2012]. Because the correction for changing $Mg/Ca_{sw}$ is not linear, we include the species-specific power-law exponential H-value of 0.41 [*Delaney et al.*, 1985; *Evans and Müller*, 2012; *Evans et al.*, 2016]. $Mg/Ca_{sw}$ data are from *Fantle and dePaolo* [2006], which is consistent with $Mg/Ca_{sw}$ estimates from marine evaporite fluid inclusions [*Horita et al.*, 2002; *Brennan et al.*, 2013]. Sediment was not available for 5 out of the 42 samples in the record; SST was estimated by extrapolation from new *T. sacculifer* measurements (filled black circles). The correction for dissolution with depth [*Dekens et al.*, 2002] is omitted in favor of the calibration of *Anand et al*. [2003] as water depth at this core location (2839 m) is well above the tropical Atlantic lysocline (4200 m) and bottom waters are supersaturated with respect to calcite ($\Omega = 1.5$). The original SST record (red circles) was based on *T. sacculifer* from a smaller size fraction (315-400 µm), a modern $Mg/Ca_{sw}$ value of 4.96 mmol/mol, and the depth-based dissolution correction of *Dekens et al*. [2002], which resulted in ~1.8 K warmer calculated SST. Modern SST reconstructed from core top material [*Henehan et al.*, 2013] and from annual average climatology (WOAS) is plotted for comparison.

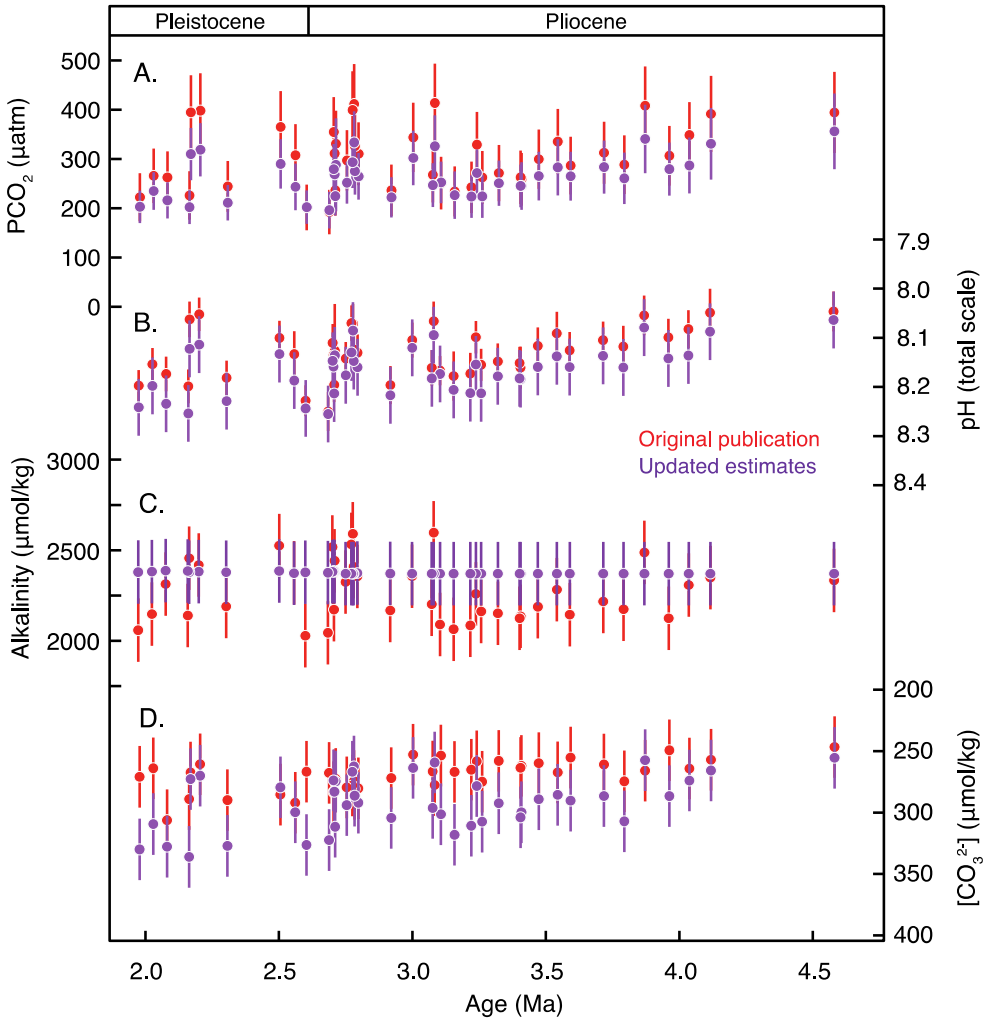


**Figure S5**. Original paleoceanographic estimates (red symbols) from *Bartoli et al*. [2011] compared with updated estimates (purple symbols) for (A) $PCO_2$, (B) pH, (C) total alkalinity, and (D) carbonate ion concentration, [$CO_3^{2-}$]. The original publication paired pH with carbonate ion concentration estimates as input parameters for the carbonate system whereas this study uses estimates of total alkalinity as the second parameter. Using pH and alkalinity as inputs reduces the $PCO_2$ variability compared to the original estimate. Furthermore, if $PCO_2$ is calculated using [$CO_3^{2-}$] as the second parameter, the corresponding alkalinity widely varies over a range of ~800 µmol/kg, which highlights the greater sensitivity of calculated $PCO_2$ in (A) to small uncertainties in [$CO_3^{2-}$]. Such a large variability in alkalinity is unreasonable given geochemical modelling constraints [*Tyrrell and Zeebe*, 2004; *Ridgwell*, 2005] and the limited range of late Pleistocene alkalinity (~120 µmol/kg) [*Clark et al.*, 2006] due to the stabilizing effect on alkalinity from the distribution of calcium carbonate accumulation in the deep sea.

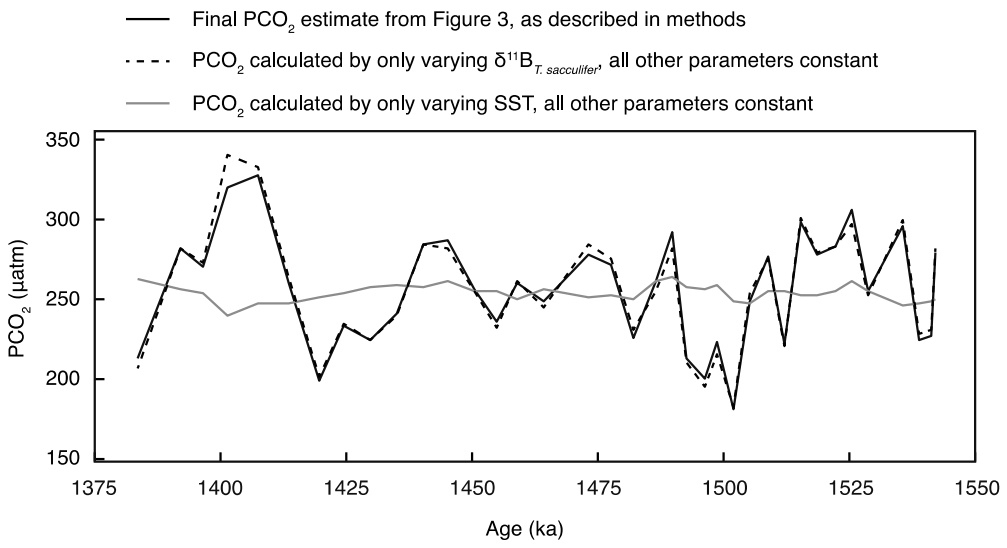


**Figure S6**. Sensitivity study of contributing factors to $PCO_2$ calculations (Site 668B, this study). (A) The primary component of calculated $PCO_2$ is the initial $\delta^{11}B$ measurement input. Here the final $PCO_2$ estimate (from Figure 3) is plotted alongside $PCO_2$ calculated by varying only the measured $\delta^{11}B_{T.\ sacculifer}$ values and keeping all other parameters constant (dashed line). The second greatest contributor to calculated $PCO_2$ uncertainty is SST. However, if $pCO_2$ is calculated by only varying SST, the maximum $pCO_2$ range is minimized to only ~24 µatm (grey solid line).

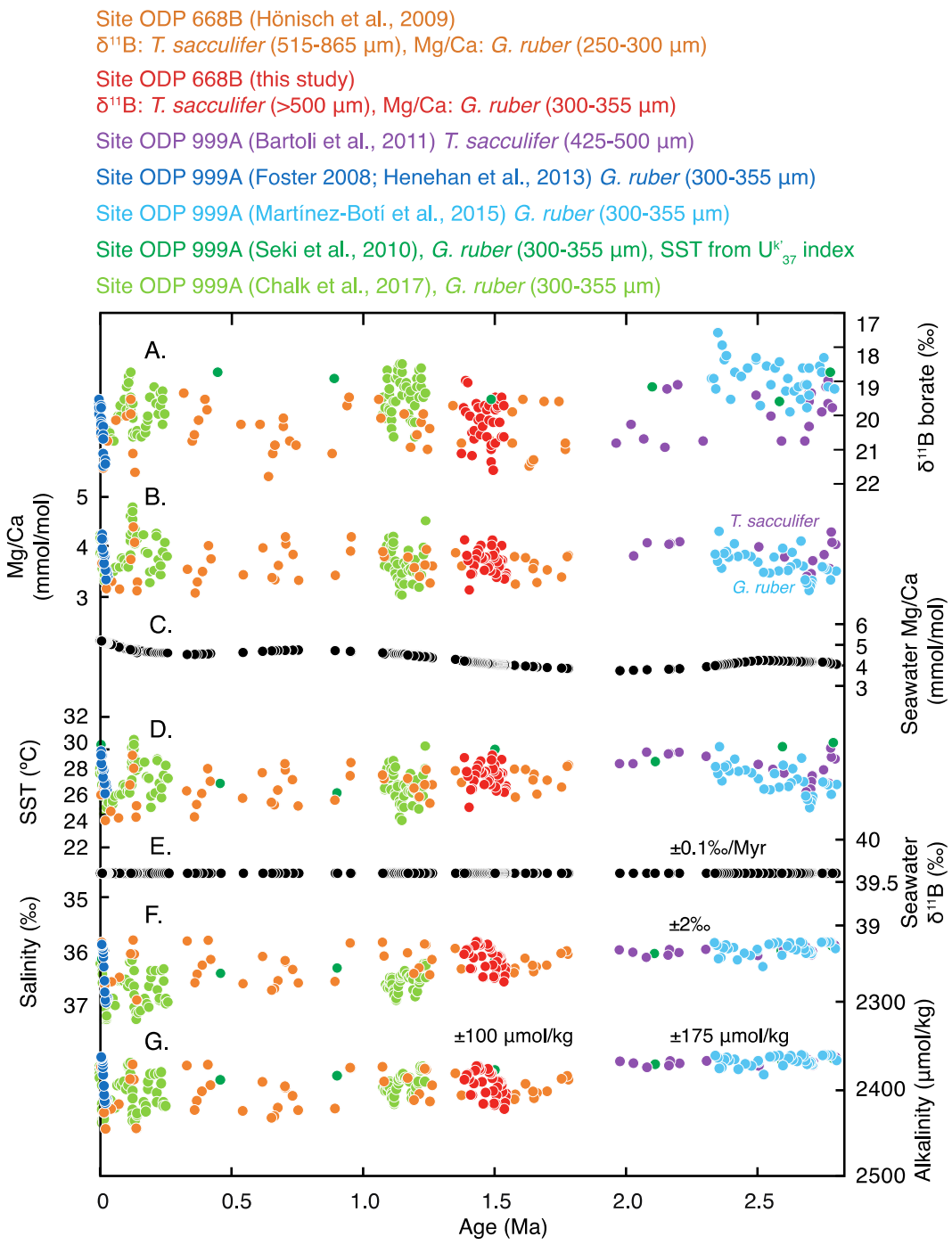


**Figure S7**. Supplemental data for $pCO_2$ calculations in Figure 4, differentiated by $\delta^{11}B$ source: dark blue [*Henehan et al.*, 2013], orange [*Hönisch et al.*, 2009], red (this study), purple [*Bartoli et al.*, 2011], light blue [*Martínez-Botí et al.*, 2015] and green [*Seki et al.*, 2010]. (A) Borate $\delta^{11}B$ calculated from foraminiferal $\delta^{11}B$ of foraminifera and analytical technique-specific calibrations (see Methods for details). (B) Mg/Ca data are used for SST reconstructions and are based on *G. ruber*, 250-300 µm (orange), *G. ruber*, 300-355 µm (red), *T. sacculifer*, 425-500 µm (purple) and *G. ruber*, 300-355 µm [*Henehan et al.*, 2013; *Martínez-Botí et al.*, 2015]. (C) The Mg/Ca value

of seawater (used for correcting Mg/Ca-based SST) is taken from *Fantle and DePaolo* [2006], which for this time period is consistent with $Mg/Ca_{sw}$ estimates from marine evaporite fluid inclusions [*Horita et al.*, 2002; *Brennan et al.*, 2013]. (D) SST is based on Mg/Ca data and corrected for changes in $Mg/Ca_{sw}$ [*Evans and Müller*, 2012] in all cases, except *Seki et al*. [2010] who based their SST estimates on the alkenone unsaturation index ($U^{k'}_{37}$). (E) The $\delta^{11}B$ value of seawater is assumed to have been constant over the past 5 Ma (F) Salinity at Site 668B is derived from the modeled sea level estimates of *Bintanja and van de Wal* [2008] as described in the text, with an uncertainty of ±2‰. (G) Alkalinity calculated using local S:ALK relationship of $TA_{668B}$ = 65.62*S+22.84 and $TA_{999A}$ = 59.19 + 229.08 [*Foster*, 2008], based on modern surface WOCE and GLODAP data. Alkalinity uncertainty is ±100 μmol/kg for the past 1.9 Ma and ±175 for samples older than 1.9 Ma.

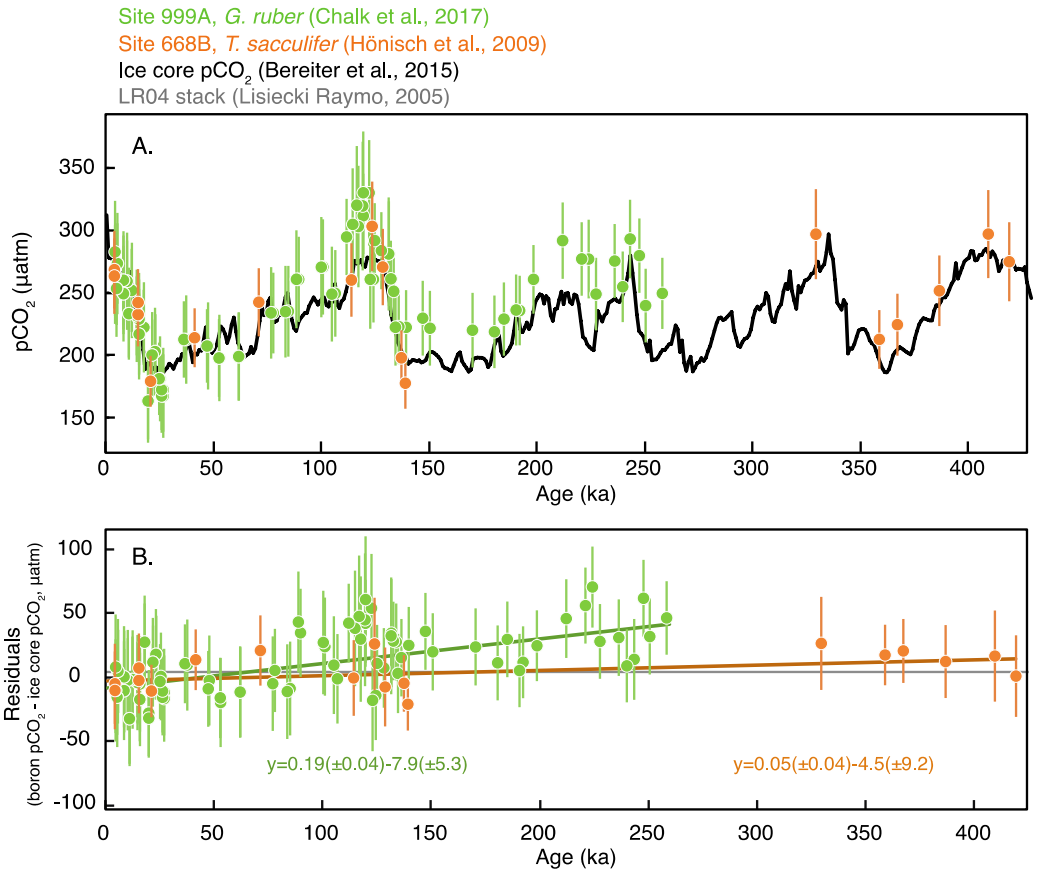


**Figure S8**. (A) Expanded view of boron-based $pCO_2$ from Figure 7, as calculated using the published $\delta^{11}B$ measurements [*Hönisch et al.*, 2009; *Chalk et al.*, 2017] and the boundary conditions set forth in the Methods, compared with $pCO_2$ from ice core measurements [*Bereiter et al.*, 2015]. (B) Difference between boron-based $pCO_2$ and ice core $pCO_2$. Over the past 260 ka, the difference between *G. ruber*-based $pCO_2$ and ice core $pCO_2$ is larger further back in time, which we suggest is most likely due to small evolutionary changes in *G. ruber* ecology or habitat over time.

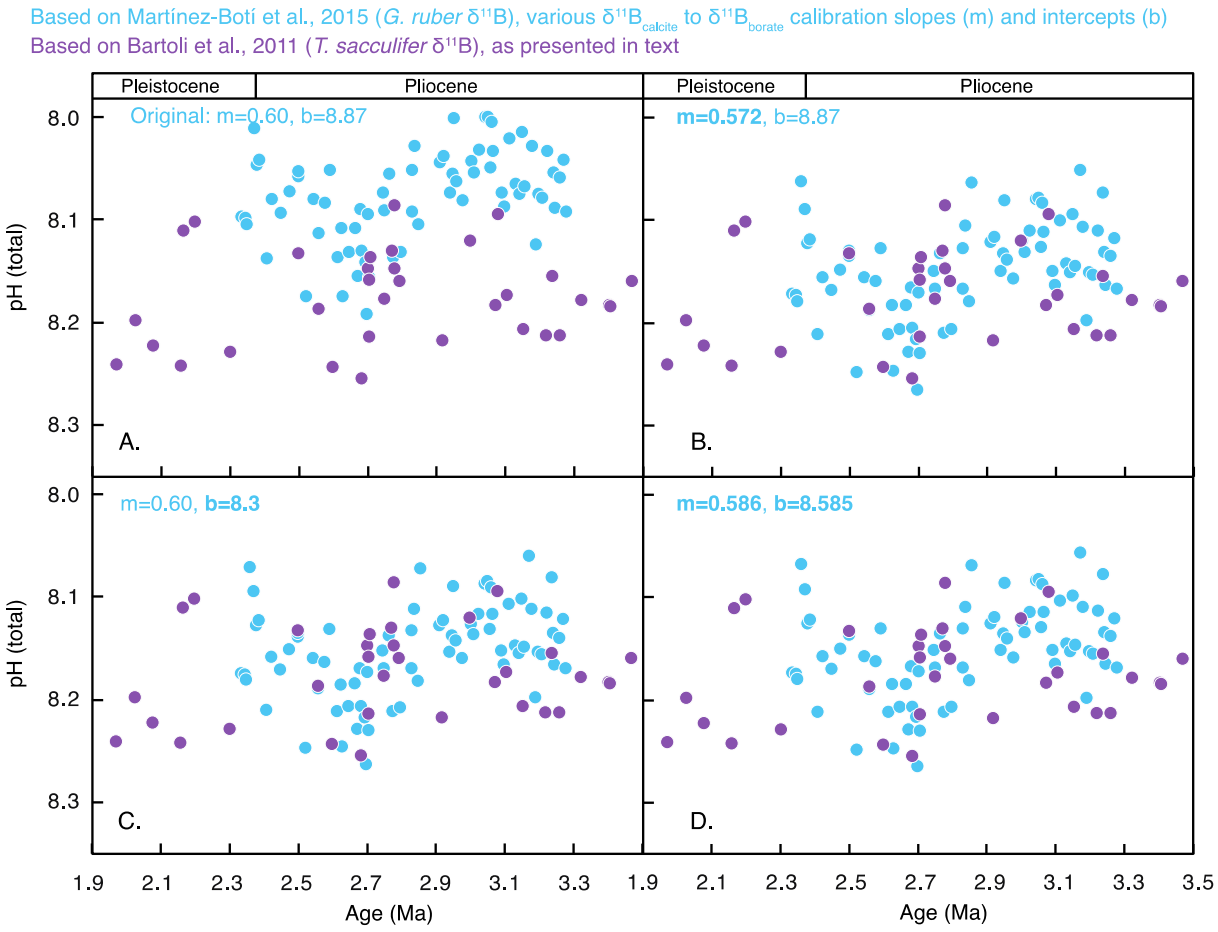


**Figure S9**. If we assume that the *T. sacculifer*-based pH record from Site 999 is correct for the early Pleistocene-late Pliocene, the pH offset of the *G. ruber*-based pH record from Site 999 from the same time period could be due to a biologically-mediated change in the slope and/or intercept of the *G. ruber* $\delta^{11}B_{calcite}$ to $\delta^{11}B_{borate}$ relationship. The modern *G. ruber* $\delta^{11}B_{calcite}$ to $\delta^{11}B_{borate}$ calibration has a slope of 0.60 and intercept of 8.87 [*Henehan et al.*, 2013]; if the *G. ruber* calibration slope is modified to force the two pH records to match, then the new Plio-Pleistocene slope for *G. ruber* samples would become 0.572 (panel B). If instead the intercept is modified to force a match, the new intercept is 8.3 (panel C). A number of potential matches can be made by changing both the calibration slope and intercept; a third example of one of these potential solutions is given in panel D.

**Table S1**. Data from Figure 2. Calibration of $\delta^{11}B$ of *T. sacculifer* (>450 μm) to $\delta^{11}B$ of seawater borate ion as measured via N-TIMS for down-core records.

**Culture**

| pH[1] | $\delta^{11}B$ (‰) | $\delta^{11}B$ 2se | $\delta^{11}B$ borate (‰) [3] | $\delta^{11}B$ borate uncertainty [4] | Temp. (ºC) | Sal. | Reference |
|---|---|---|---|---|---|---|---|
| 7.49 | 17.68 | 0.8 | 14.18 | 0.22 | 27 | 35.4 | *Sanyal et al.*, 2001 [2] |
| 8.03 | 20.69 | 0.25 | 18.20 | 0.66 | 27 | 35.4 | [5] |
| 8.07 | 20.71 | 0.7 | 18.65 | 0.58 | 27 | 35.4 | *Sanyal et al.*, 2001 [2] |
| 8.45 | 24.40 | 0.21 | 23.89 | 0.47 | 27 | 35.4 | [5] |
| 8.47 | 25.85 | 0.5 | 24.20 | 0.78 | 27 | 35.4 | *Sanyal et al.*, 2001 [2] |

**Core top**

| pH[1] | $\delta^{11}B$ (‰) | $\delta^{11}B$ 2se | $\delta^{11}B$ borate (‰) [3] | $\delta^{11}B$ borate uncertainty [4] | Temp. (ºC) | Sal. | Reference |
|---|---|---|---|---|---|---|---|
| 8.17 | 20.84 | 0.34 | 19.97 | 0.04 | 27.72 | 35.25 | ODP 668B, *Hönisch et al*., 2009 |
| 8.12 | 20.80 | 0.22 | 19.36 | 0.04 | 25.8 | 40.02 | GeoB 5810 [6] |
| 8.14 | 20.66 | 0.28 | 19.69 | 0.04 | 29.14 | 34.3 | RC10-139, *Hönisch and Hemming*, 2004 |
| 8.14 | 20.49 | 0.19 | 19.61 | 0.04 | 28.45 | 34.42 | V34-54, *Hönisch and Hemming*, 2004 |
| 8.07 | 20.42 | 0.19 | 18.77 | 0.03 | 27.63 | 35.82 | ODP 999A [6] |

**Core top details**

| Core | Latitude | Longitude | Sample | *T. sacculifer* size fraction (μm) |
|---|---|---|---|---|
| GeoB 5810 | 29.56ºN | 35.02ºE | 10-20 cm | 450-500 |
| ODP 999A | 12.75ºN | 78.73ºW | 1-1, 3-5 cm | 515-865 |

[1] All pH values on the total scale.
[2] Culture studies corrected for $\delta^{11}B_{sw}$ where $\delta^{11}B_{sw}$ was different from 39.61‰. *Sanyal et al*. [2001]. In addition, *T. sacculifer* $\delta^{11}B$ data from an old NBS 6" radius of curvature NTIMS at SUNY Stony Brook corrected by -1.1‰ to be equivalent with $\delta^{11}B$ measured on the Triton at LDEO [*Hönisch et al*., 2009].
[3] $\delta^{11}B$ of borate calculated using $\alpha_{B3\text{-}B4}$ after *Klochko et al*. [2006] and T, S effects on pK*B after *Dickson* [1990] and *Millero* [1995], with constants corrected after *Rae et al*. [2011] and the isotopic composition of borate calculated using the revised boron isotope mass balance of *Rae* [2018].
[4] The uncertainty in $\delta^{11}B_{borate}$ is based on the pH uncertainty only and does not take into account uncertainties in temperature and salinity.
[5] New cultured *T. sacculifer* data are based on specimens cultured in Puerto Rico in 2010 using methods identical to *Allen et al*. [2012]. Both samples were analyzed on the Triton TIMS at LDEO using established analytical [*Hönisch et al*., 2009] and cleaning methods [*Russell et al*., 2004].
[6] Core top $\delta^{11}B$ measurements are carried out with the same technique as described in the text, section 2.1. Core locations and samples are described above.

**Table S2**. Summary of peak marine isotope stages (MIS) used to define average data for cross plots and maximum and minimum $pCO_2$ estimated for each stage.

| MIS | Start age (ka) | End age (ka) | Age (ka) | Glacial $pCO_2$ (μatm) | Interglacial $pCO_2$ (μatm) | Comment |
|---|---|---|---|---|---|---|
| 44 | 1370 | 1385 | 1384 | 214 | | MIS 44 min |
| 45 | 1395 | 1410 | 1397 | | 271 | |
| | | | 1402 | | 320 | |
| | | | 1408 | | 327 | MIS 45 max |
| 46 | 1415 | 1426 | 1420 | 201 | | MIS 46 min |
| | | | 1425 | 234 | | |
| 47 | 1436 | 1450 | 1441 | | 285 | MIS 47 max |
| | | | 1446 | | 287 | |
| 48 | 1454 | 1467 | 1456 | 237 | | MIS 48 min |
| | | | 1459 | 261 | | |
| | | | 1465 | 249 | | |
| 49 | 1485 | 1491 | 1487 | | 262 | |
| | | | 1490 | | 292 | MIS 49 max |
| 50 | 1495 | 1504 | 1496 | 201 | | |
| | | | 1499 | 224 | | |
| | | | 1502 | 183 | | MIS 50 min |
| 51 | 1514 | 1527 | 1516 | | 299 | |
| | | | 1519 | | 278 | |
| | | | 1522 | | 284 | |
| | | | 1526 | | 306 | MIS 51 max |
| 52 | 1537 | 1542 | 1539 | 226 | | MIS 52 min |
| | | | 1541 | 228 | | |

**Supporting Information Reference List**


Allen, K. A., B. Hönisch, S. M. Eggins, and Y. Rosenthal (2012), Environmental controls on B/Ca in calcite tests of the tropical planktic foraminifer species *Globigerinoides ruber* and *Globigerinoides sacculifer*, *Earth and Planetary Science Letters*, *351-352*(C), 270–280, doi:10.1016/j.epsl.2012.07.004.

Anand, P., H. Elderfield, and M. H. Conte (2003), Calibration of Mg/Ca thermometry in planktonic foraminifera from a sediment trap time series, *Paleoceanography*, *18*(2), 1050, doi:10.1029/2002PA000846.

Bartoli, G., B. Hönisch, and R. E. Zeebe (2011), Atmospheric $CO_2$ decline during the Pliocene intensification of Northern Hemisphere glaciations, *Paleoceanography*, *26*(4), PA3206, doi:10.1029/2010PA002055.

Bemis, B. E., H. J. Spero, J. Bijma, and D. W. Lea (1998), Reevaluation of the oxygen isotopic composition of planktonic foraminifera: Experimental results and revised paleotemperature equations, *Paleoceanography*, *13*(2), 150–160, doi:10.1029/98PA00070.

Bereiter, B., S. Eggleston, J. Schmitt, C. Nehrbass-Ahles, T. F. Stocker, H. Fischer, S. Kipfstuhl, and J. Chappellaz (2015), Revision of the EPICA Dome C CO2 record from 800 to 600kyr before present, *Geophysical Research Letters*, *42*(2), 542–549, doi:10.1002/2014GL061957.

Bintanja, R., and R. S. W. van de Wal (2008), North American ice-sheet dynamics and the onset of 100,000-year glacial cycles, *Nature*, *454*(7206), 869–872, doi:10.1038/nature07158.

Brennan, S. T., T. K. Lowenstein, and D. I. Cendon (2013), The major-ion composition of Cenozoic seawater: The past 36 million years from fluid inclusions in marine halite, *American Journal of Science*, *313*(8), 713–775, doi:10.2475/08.2013.01.

Chalk, T. B. et al. (2017), Causes of ice age intensification across the Mid-Pleistocene Transition, *PNAS*, *114*(50), 13114–13119, doi:10.1073/pnas.1702143114.

Clark, P. U., D. Archer, D. Pollard, J. D. Blum, J. A. Rial, V. Brovkin, A. C. Mix, N. G. Pisias, and M. Roy (2006), The middle Pleistocene transition: characteristics, mechanisms, and implications for long-term changes in atmospheric $pCO_2$, *Quaternary Science Reviews*, *25*(23-24), 3150–3184, doi:10.1016/j.quascirev.2006.07.008.

Dekens, P. S., D. W. Lea, D. K. Pak, and H. J. Spero (2002), Core top calibration of Mg/Ca in tropical foraminifera: Refining paleotemperature estimation, *Geochemistry Geophysics Geosystems*, *3*, 1022, doi:10.1029/2001GC000200.

Delaney, M. L., A. W. H. Bé, and E. A. Boyle (1985), Li, Sr, Mg, and Na in foraminiferal calcite shells from laboratory culture, sediment traps, and sediment cores, *Geochimica et Cosmochimica Acta*, doi:10.1016/0016-7037(85)90284-4.

Dickson, A. G. (1990), Thermodynamics of the dissociation of boric acid in synthetic seawater from 273.15 to 318.15 K, *Deep-Sea Research II*, *37*, 755–766, doi:10.1021/je00061a009.

Evans, D., and W. Müller (2012), Deep time foraminifera Mg/Ca paleothermometry: Nonlinear correction for secular change in seawater Mg/Ca, *Paleoceanography*, *27*(4), PA4205, doi:10.1029/2012PA002315.

Evans, D., C. M. Brierley, M. E. Raymo, J. Erez, and W. Müller (2016), Planktic foraminifera shell chemistry response to seawater chemistry: Pliocene–Pleistocene seawater Mg/Ca, temperature and sea level change, *Earth and Planetary Science Letters*, *438*(C), 139–148, doi:10.1016/j.epsl.2016.01.013.

Fantle, M. S., and D. J. DePaolo (2006), Sr isotopes and pore fluid chemistry in carbonate sediment of the Ontong Java Plateau: Calcite recrystallization rates and evidence for a rapid rise in seawater Mg over the last 10 million years, *Geochimica et Cosmochimica Acta*, *70*(15), 3883–3904.

Foster, G. L. (2008), Seawater pH, $pCO_2$ and $[CO_3^{-2}]$ variations in the Caribbean Sea over the last 130 kyr: A boron isotope and B/Ca study of planktic foraminifera, *Earth and Planetary Science Letters*, *271*(1-4), 254–266, doi:10.1016/j.epsl.2008.04.015.

Foster, G. L., P. A. E. Pogge von Strandmann, and J. W. B. Rae (2010), Boron and magnesium isotopic composition of seawater, *Geochemistry Geophysics Geosystems*, *11*(8), doi:10.1029/2010GC003201.

Greenop, R., M. P. Hain, S. M. Sosdian, K. I. C. Oliver, P. Goodwin, T. B. Chalk, C. H. Lear, P. A. Wilson, and G. L. Foster (2017), A record of Neogene seawater $\delta^{11}B$ reconstructed from paired $\delta^{11}B$ analyses on benthic and planktic foraminifera, *Climate of the Past*, *13*(2), 149–170, doi:10.5194/cp-13-149-2017.

Groeneveld, J. (2005), Effect of the Pliocene closure of the Panamanian Gateway on Caribbean and east Pacific sea surface temperatures and salinities by applying combined Mg/Ca and, 1–165 pp. Christian Albrechts University, 20 October.

Hansen, J., M. Sato, G. Russell, and P. Kharecha (2013), Climate sensitivity, sea level and atmospheric carbon dioxide, *Philosophical Transactions of the Royal Society A: Mathematical, Physical and Engineering Sciences*, *371*(2001), 20120294–20120294, doi:10.1666/0094-8373(2000)26[259:GCCANA]2.0.CO;2.

Henehan, M. J. et al. (2013), Calibration of the boron isotope proxy in the planktonic foraminifera *Globigerinoides ruber* for use in palaeo-$CO_2$ reconstruction, *Earth and Planetary Science Letters*, *364*, 111–122, doi:10.1016/j.epsl.2012.12.029.

Horita, J., H. Zimmermann, and H. D. Holland (2002), Chemical evolution of seawater during the Phanerozoic: Implications from the record of marine evaporites, *Geochimica et Cosmochimica Acta*, *66*(21), 3733–3756, doi:10.1016/S0016-7037(01)00884-5.

Hönisch, B., and N. G. Hemming (2004), Ground-truthing the boron isotope-paleo-pH proxy in planktonic foraminifera shells: Partial dissolution and shell size effects, *Paleoceanography*, *19*(4), PA4010, doi:10.1029/2004PA001026.

Hönisch, B., N. G. Hemming, D. Archer, M. Siddall, and J. F. McManus (2009), Atmospheric carbon dioxide concentration across the mid-Pleistocene transition, *Science*, *324*(5934), 1551, doi:10.1126/science.1171477.

Klochko, K., A. J. Kaufman, W. Yao, R. H. Byrne, and J. A. Tossell (2006), Experimental measurement of boron isotope fractionation in seawater, *Earth and Planetary Science Letters*, *248*(1-2), 276–285, doi:10.1016/j.epsl.2006.05.034.

Lemarchand, D., J. Gaillardet, E. Lewin, and C. J. Allegre (2000), The influence of rivers on marine boron isotopes and implications for reconstructing past ocean pH, *Nature*, *408*(6815), 951–954, doi:10.1038/35050058.

Lisiecki, L. E., and M. E. Raymo (2005), A Pliocene-Pleistocene stack of 57 globally distributed benthic $\delta^{18}O$ records, *Paleoceanography*, *20*, doi:10.1029/2004PA001071.

Martin, P. A., and D. W. Lea (2002), A simple evaluation of cleaning procedures on fossil benthic foraminiferal Mg/Ca, *Geochemistry Geophysics Geosystems*, *3*(10), 1–8, doi:10.1029/2001GC000280.

Martínez-Botí, M. A., G. L. Foster, T. B. Chalk, E. J. Rohling, P. F. Sexton, D. J. Lunt, R. D. Pancost, M. P. S. Badger, and D. N. Schmidt (2015), Plio-Pleistocene climate sensitivity evaluated using high-resolution $CO_2$ records, *Nature*, *518*(7537), 49–54, doi:10.1038/nature14145.

Medina-Elizalde, M., D. W. Lea, and M. S. Fantle (2008), Implications of seawater Mg/Ca variability for Plio-Pleistocene tropical climate reconstruction, *Earth and Planetary Science Letters*, *269*(3-4), 585–595, doi:10.1016/j.epsl.2008.03.014.

Millero, F. J. (1995), Thermodynamics of the carbon dioxide system in the oceans, *Geochimica et Cosmochimica Acta*, *59*(4), 661–677, doi:10.1016/0016-7037(94)00354-o.

Paillard, D., L. Labeyrie, and P. Yiou (1996), Macintosh Program performs time-series analysis, *Eos Trans. AGU*, *77*(39), 379–379, doi:10.1029/96EO00259.

Pearson, P. N., and M. Palmer (2000), Atmospheric carbon dioxide concentrations over the past 60 million years, *Nature*, *406*(6797), 695–699, doi:10.1038/35021000.

Rae, J. W. B. (2018), Boron Isotopes in Foraminifera: Systematics, Biomineralisation, and $CO_2$ Reconstruction, in *Boron Isotopes*, vol. 55, pp. 107–143, Springer International Publishing, Cham, Switzerland.

Rae, J. W. B., G. L. Foster, D. N. Schmidt, and T. Elliott (2011), Boron isotopes and B/Ca in benthic foraminifera: Proxies for deep ocean carbonate system, *Earth and Planetary Science Letters*, *302*(3-4), 403–413, doi:10.1016/j.epsl.2010.12.034.

Raitzsch, M., and B. Hönisch (2013), Cenozoic boron isotope variations in benthic foraminifers, *Geology*, *41*(5), 591–594, doi:10.1130/G34031.1.

Ridgwell, A. (2005), A Mid Mesozoic Revolution in the regulation of ocean chemistry, *Marine Geology*, *217*(3-4), 339–357, doi:10.1016/j.margeo.2004.10.036.

Russell, A.D., Hönisch, B., Spero, H.J., and D. W. Lea (2004), Effects of seawater carbonate ion concentration and temperature on shell U, Mg, and Sr in cultured planktonic foraminifera, *Geochimica et Cosmochimica Acta*, *68*(21), 4347–4361, doi: 10.1016/j.gca.2004.03.013.

Sanyal, A., J. Bijma, H. J. Spero, and D. W. Lea (2001), Empirical relationship between pH and the boron isotopic composition of *Globigerinoides sacculifer*: Implications for the boron isotope paleo-pH proxy, *Paleoceanography*, *16*(5), 515–519, doi:10.1029/2000pa000547.

Schmidt, M., H. J. Spero, and D. W. Lea (2004), Links between salinity variation in the Caribbean and North Atlantic thermohaline circulation, *Nature*, *428*, 160–163, doi:10.1038/nature02346.

Schmidt, G. A. et al. (2017), Overestimate of committed warming, *Nature*, *547*(7662), E16–E17, doi:10.1038/nature22803.

Seki, O., G. L. Foster, D. N. Schmidt, A. Mackensen, K. Kawamura, and R. D. Pancost (2010), Alkenone and boron-based Pliocene $pCO_2$ records, *Earth and Planetary Science Letters*, *292*(1-2), 201–211, doi:10.1016/j.epsl.2010.01.037.

Shackleton, N. J., A. L. Berger, and W. Peltier (1990), An alternative astronomical calibration of the lower Pleistocene timescale based on ODP Site 677, *Trans. R. Soc. Edinburgh Earth Sci*, *81*, 251–261, doi:10.1017/s0263593300020782.

Shipboard Scientific Party (1988), Site 668, in *Proceedings of the Ocean Drilling Program, Initial Reports*, vol. 108, edited by W. Ruddiman, M. Sarnthein, J. Baldauf, et al., pp. 931–946, Ocean Drilling Program, College Station, TX.

Steph, S., R. Tiedemann, M. Prange, J. Groeneveld, D. Nürnberg, L. Reuning, M. Schulz, and G. H. Haug (2006), Changes in Caribbean surface hydrography during the Pliocene shoaling of the Central American Seaway, *Paleoceanography*, *21*(4), 1–25, doi:10.1029/2004PA001092.

Tyrrell, T., and R. E. Zeebe (2004), History of carbonate ion concentration over the last 100 million years, *Geochimica et Cosmochimica Acta*, *68*(17), 3521–3530, doi:10.1016/j.gca.2004.02.018.